Physics of Plasmas

Generation of harmonic Alfvén waves and its implications to heavy ion heating in the solar corona: Hybrid simulations

Cite as: Phys. Plasmas **27**, 012901 (2020); https://doi.org/10.1063/1.5126169
Submitted: 31 August 2019 . Accepted: 04 December 2019 . Published Online: 02 January 2020

Jiansheng Yao, Quanming Lu, Xinliang Gao, Jian Zheng, Huayue Chen, Yi Li, and Shui Wang

Physics of Plasmas ARTICLE scitation.org/journal/php

Generation of harmonic Alfvén waves and its implications to heavy ion heating in the solar corona: Hybrid simulations

Cite as: Phys. Plasmas **27**, 012901 (2020); doi: 10.1063/1.5126169
Submitted: 31 August 2019 · Accepted: 4 December 2019 ·
Published Online: 2 January 2020

Jiansheng Yao,[1,2] Quanming Lu,[1,2,a)] Xinliang Gao,[1,2] Jian Zheng,[3] Huayue Chen,[1,2] Yi Li,[1,2] and Shui Wang[1,2]

AFFILIATIONS

[1]CAS Key Lab of Geospace Environment, School of Earth and Space Sciences, University of Science and Technology of China, Hefei 230026, China
[2]CAS Center for Excellence in Comparative Planetology, Hefei 230026, China
[3]CAS Key Lab of Geospace Environment, School of Physical Sciences, University of Science and Technology of China, Hefei 230026, China

[a)]Author to whom correspondence should be addressed: qmlu@ustc.edu.cn

ABSTRACT

Harmonic Alfvén waves in the magnetosphere have been reported by recent observation [Chen *et al.,* Astrophys. J. **859**, 120 (2018)]. In this paper, one-dimensional hybrid simulations are performed to investigate the generation of harmonic Alfvén waves. We find that when Alfvén waves propagate obliquely with respect to the ambient magnetic field, electrostatic components (or equivalently the density fluctuations) emerge, and their coupling with the electromagnetic field associated Alfvén waves leads to the harmonics of Alfvén waves. These high-frequency harmonic Alfvén waves can resonantly interact with heavy ions when the cyclotron resonant condition is satisfied and preferentially heat heavy ions in the perpendicular direction. The implications to solar coronal heating are also discussed in the paper.

Published by AIP Publishing. https://doi.org/10.1063/1.5126169

I. INTRODUCTION

The temperature of the solar corona is 2–3 orders higher than that of the photosphere, and how the corona is heated is still one of the biggest challenges in solar physics.[2–5] Based on the observations by UVCS (ultraviolet coronagraph spectrometer) and SUMER (solar ultraviolet measurements of emitted radiation) on the SOHO (solar and heliospheric observatory), the preferential heating of heavy oxygen ions O^{5+} over protons has been revealed.[4,6] Furthermore, during this process, a strong temperature anisotropy with $T_\perp > T_{||}$ (here, $||$ and $\perp$ are the directions parallel and perpendicular to the ambient magnetic field, respectively) has also been identified.[6–9] The physical mechanism underlying these phenomena should give us a crucial clue to explain the long-standing puzzle on how the solar corona is efficiently heated.

Alfvén waves, which are omnipresent in the solar corona and solar wind,[10] are believed to be the most promising candidate for heating the solar corona and solar wind. In general, the frequencies of the Alfvén waves in the solar corona are considered to be much lower than the ion cyclotron frequency. One possible mechanism to heat the solar corona is ion stochastic heating or nonresonant heating by low-frequency Alfvén waves with sufficiently large amplitudes.[11–14] Another school of thought[15–22] is that the low-frequency Alfvén waves can produce high-frequency resonant waves via turbulent cascade. However, just as mentioned by previous researchers,[23–27] the classical magnetohydrodynamics (MHD) turbulence scenario has a serious flaw: MHD turbulence tends to produce large cross-field wavenumbers $k_\perp$, but cyclotron resonance needs large parallel wavenumbers $k_{||}$. Therefore, it is impossible for MHD turbulence to heat heavy ions via cyclotron resonance, but simulations of MHD turbulence[28–31] have revealed that ions are efficiently heated in the perpendicular direction. Thus, mechanisms other than cyclotron resonance are necessary for interpreting the heating of ions by MHD turbulence. Further investigations showed that this heating is highly intermittent and close related to strong current density,[30] and some studies[31] proposed that the heating may be related to the small-scale transverse electric fields produced by the transverse motion of electron holes. However, these heating mechanisms of MHD turbulence are so sophisticated and far beyond the scope of this paper, and we still regard cyclotron resonance as the main mechanism to heat heavy ions in the perpendicular direction in this paper. Hence, searching mechanisms that can produce large parallel wavenumbers $k_{||}$ needed for cyclotron resonance is still important to study the heating of the solar wind and solar corona.

In this paper, through performing one-dimensional (1-D) hybrid simulations, we find that obliquely propagating Alfvén waves can couple with the associated density fluctuations in the wave propagating direction, which generates harmonic Alfvén waves with large values of $k_{\parallel}$. The implications of this mechanism on the heating of heavy ions are also discussed.

This paper is organized as follows. In Sec. II, the hybrid simulation model and initial condition are given. The simulation results are presented in Sec. III. A summary and discussion of the results are presented in Sec. IV.

II. SIMULATION MODEL

A one-dimensional (1-D) hybrid simulation model is used to investigate the generation of harmonic Alfvén waves and subsequent heating of heavy ions. In the hybrid simulation model, ions are treated as particles and move with the action of the Lorentz force. Electrons are considered as massless fluid.[32–34]

In the 1-D hybrid simulations, all physical variables can only change along the x direction, and the background magnetic field is $\mathbf{B}_0 = B_0 \cos\theta \mathbf{i}_x + B_0 \sin\theta \mathbf{i}_y$, where θ is the angle within the propagating direction and x-axis. The dispersion relation of the Alfvén waves can be obtained according to the Hall magnetohydrodynamical (Hall-MHD) equations if the fluctuations associated with the Alfvén waves are sufficiently small, and it can be described as follows:

$$\Omega_p^2(2k^2v_A^2\cos^2\theta\omega^2 + k^2v_A^2\sin^2\theta\omega^2 - k^4v_A^4\cos^2\theta - \omega^4) + k^4v_A^4\cos^2\theta\omega^2 = 0, \tag{1}$$

where $v_A = B_0/\sqrt{\mu_0\rho_0}$ (ρ_0 is the ambient plasma density and μ_0 is the permeability of vacuum), $\Omega_p = qB_0/m_i$ is the proton cyclotron frequency, and ω and k are the frequency and wavenumber of the Alfvén waves, respectively. When the frequency of the Alfvén waves is much smaller than that of the proton cyclotron waves, the dispersion relation can be reduced to $\omega^2 = k^2v_A^2\cos^2\theta$.

Also, we can get the following equation describing the fluctuating plasma density $\delta\rho$ and fluctuating magnetic field $\delta\mathbf{B}$:

$$\delta B_y = \frac{i\Omega_p\left(\frac{k^2v_A^2}{\omega}\cos^2\theta - \omega\right)}{k_x^2v_A^2\cos\theta}\delta B_z, \tag{2}$$

$$\delta\rho = i\frac{\sin\theta\Omega_p\left(k^2\cos^2\theta v_A^2 - \omega^2\right)}{\omega^3\cos^2\theta}\frac{\delta B_z}{B_0}\rho_0. \tag{3}$$

It indicates that the fluctuating density $\delta\rho$ will disappear when the wave propagates along the background magnetic field ($\theta = 0$). The fluctuating bulk velocities $\mathbf{\delta u}$ associated with the Alfvén waves are

$$\delta u_x = \frac{k_xv_A^2\sin\theta}{\omega}\frac{\delta B_y}{B_0}, \tag{4}$$

$$\delta u_y = -\frac{k_xv_A^2\cos\theta}{\omega}\frac{\delta B_y}{B_0}, \tag{5}$$

$$\delta u_z = -\frac{k_xv_A^2\cos\theta}{\omega}\frac{\delta B_z}{B_0}. \tag{6}$$

In the simulations, the units of length and time are the proton inertial length $d_i = c/\omega_{pp}$ (c and ω_{pp} are the light speed and proton plasma frequency, respectively) and the inverse of the proton gyrofrequency Ω_p^{-1}. Therefore, the plasma velocity is normalized to v_A. The number of grids is $n_x = 2000$, and each size is $\Delta x = 1.0d_i$. The time step is $\Delta t = 0.025\,\Omega_p^{-1}$. The average proton number in each cell is 1200. The electron resistive length is set as $L_r = \eta c^2/(4\pi v_A) = 0.02c/\omega_{pp}$ (where η is the electron resistivity). The proton beta is $\beta_p = 0.01$, which is a typical value in the solar corona. The periodic boundary condition is used in our simulations. We also study the dynamics of the heavy ions with O^{5+} to be the representative, which are the important heavy ions in the solar wind.[4,6] According to previous observations,[35,36] the abundance of O^{5+} is 3×10^{-6}; thus, O^{5+} can be treated as test particles. Just like the previous study, the thermal velocity of O^{5+} is set to be the same as that of the ambient protons.

Three runs with different parameters shown in Table I are performed in this paper. Initially, left-handed polarized Alfvén waves propagating along the x-direction are employed. The fluctuating magnetic field $\delta\boldsymbol{B}$ and bulk velocities $\delta\boldsymbol{u}$ are in the form

$$\delta\boldsymbol{B} = \sum_{k,\omega=k_0,\omega_0}^{k_n,\omega_n}\left[\delta B_{yk}\cos(kx - \omega t + \varphi_k) + \delta B_{zk}\sin(kx - \omega t + \varphi_k)\right], \tag{7}$$

$$\delta\boldsymbol{u} = \sum_{k,\omega=k_0,\omega_0}^{k_n,\omega_n}\left[\delta u_{yk}\cos(kx - \omega t + \varphi_k) + \delta u_{zk}\sin(kx - \omega t + \varphi_k) - \delta u_{xk}\cos(kx - \omega t + \varphi_k)\right], \tag{8}$$

where notations $k_0 - k_n$ and $\omega_0 - \omega_n$ denote the wavenumbers and frequencies of different pump waves, respectively. For each pump wave, the wavenumber k and frequency ω satisfy the dispersion relation expressed by Eq. (1). For different runs, the initial magnetic energy remains the same. Initial phase φ_k is a random number within the range of $[0, 2\pi]$. The initial distribution of ions is the superposition of Maxwellian distribution and bulk velocities $\delta\boldsymbol{u}$.

III. SIMULATION RESULTS

We have run three cases. In the first case, the monochromic Alfvén wave propagates obliquely to the background magnetic field with the propagating angle $\theta = 20°$; in the second case, the

TABLE I. Some initial parameters in the simulation.[a]

Parameter	Run1	Run2	Run3
θ	20°	0°	20°
kd_i	0.17	0.17	0.14, 0.16, 0.17, 0.19, and 0.20
ω/Ω_p	0.15	0.15	0.13, 0.14, 0.15, 0.17, and 0.18
$\delta B_{yk}/B_0$	0.07	0.09	0.03
$\delta B_{zk}/B_0$	0.10	0.09	0.04
$\delta u_{xk}/v_A$	0.03	0.0	0.01
$\delta u_{yk}/v_A$	0.07	0.11	0.03
$\delta u_{zk}/v_A$	0.11	0.11	0.04
$\delta\rho/\rho_0$	0.03	0.0	0.03
β_e	0.1	0.1	0.1

[a]These parameters include wave normal angle θ; plasma beta of the electron β_e; the wave number of the pump wave kd_i; the frequency of pump wave ω/Ω_p; the magnetic amplitude $\delta B_y/B_0$ and $\delta B_z/B_0$; the three components of bulk velocity $\delta V_x/V_0$, $\delta V_y/V_0$, and $\delta V_z/V_0$; and fluctuating density amplitude $\delta\rho/\rho_0$ of the pump wave.

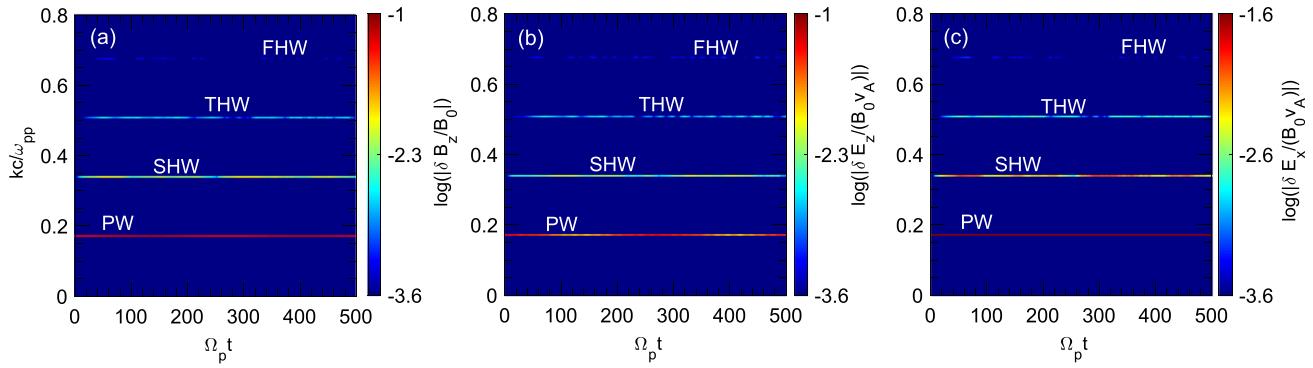

FIG. 1. The $k-t$ spectra of electromagnetic fields for run 1. (a) The $k-t$ spectrogram of perpendicular fluctuating magnetic fields ($\delta B_z/B_0$) obtained from the fast Fourier transform, (b) the $k-t$ spectrogram of perpendicular fluctuating electric fields $\delta E_z/(B_0V_A)$ obtained from the fast Fourier transform, and (c) the $k-t$ spectrogram of parallel fluctuating electric fields $\delta E_x/(B_0V_A)$. In all panels, the pump wave, its second harmonic wave, and its third harmonic wave are denoted by their acronyms "PW," "SHW," and "THW," respectively.

monochromic wave propagates along the background magnetic field with the propagating angle $\theta = 0°$. The second run performed as a comparison of the first run illustrates the influence of the propagating angle on the emergence harmonic waves. In addition, five Alfvén waves with different frequencies but the same propagating angle ($\theta = 20°$) are used in the third case to imitate the actual wave spectra with a wide range. Parameters associated with these three runs are listed in Table I. Figure 1 displays the $k-t$ spectrograms of electromagnetic fields for run 1, including (a) the $k-t$ spectrogram of magnetic field component δB_z, (b) the $k-t$ spectrogram of fluctuating electric field component δE_z, and (c) the $k-t$ spectrogram of fluctuating electric field δE_x. The pump wave, its second harmonic wave, its third harmonic wave, and the fourth harmonic wave are denoted by their acronyms "PW," "SHW," "THW," and "FHW," respectively. As shown in Fig. 1, the second harmonic wave with $kd_i \approx 2k_0d_i \approx 0.34$ begins to grow at $t = 5\,\Omega_p^{-1}$ and reaches saturation at about $t = 20\,\Omega_p^{-1}$. The third harmonic wave with $kd_i \approx 3k_0d_i \approx 0.50$ starts to appear at about $t = 20\,\Omega_p^{-1}$. After $t \approx 40\,\Omega_p^{-1}$, the fourth harmonic wave with $kd_i \approx 4k_0d_i \approx 0.68$ begins to emerge. It should be mentioned that $\delta B_x = 0$ during this process because of the Gauss theorem $\nabla \cdot \boldsymbol{B} = 0$.

Figure 2 displays the $\omega-t$ spectrograms of (a) δB_z, (b) δE_z, and (c) δE_x for run 1, respectively. It is worth noting that the sliding short-time Fourier analysis with a window size of 300 Ω_p^{-1} is employed here. In all panels, the frequency of the pump wave marked with PW is $\omega_0 \approx 0.15\,\Omega_p$ and the frequency of its second harmonic wave marked with SHW is $\omega \approx 2\omega_0 \approx 0.30\,\Omega_p$. The third harmonic wave (THW) and the fourth harmonic wave (FHW) are not presented in Fig. 2 because of insufficient resolution and their small amplitudes with the same level with noises. Thus, harmonic waves with higher frequencies having the same order of magnitude as noises in $\omega-t$ spectra will be smoothed out.

The previous observation[1] on harmonic Alfvén waves has proposed that the harmonic waves may be generated due to the coupling among the electrostatic components δE_x (or density fluctuations $\delta\rho$) and electromagnetic component δE_z. This conjecture can be verified by the corresponding bicoherence index, which has been used by many previous works[37–39] to quantitatively measure the phase coupling among three wave modes. The bicoherence index bc is defined as

$$bc = |\langle \delta E_x(k_{E_x})\delta E_z(k_{E_z})\delta E_z^*(k_{HW})\rangle|^2 / \langle |\delta E_x(k_{E_x})\delta E_z(k_{E_z})|^2\rangle \langle |\delta E_z^*(k_{HW})|^2\rangle, \quad (9)$$

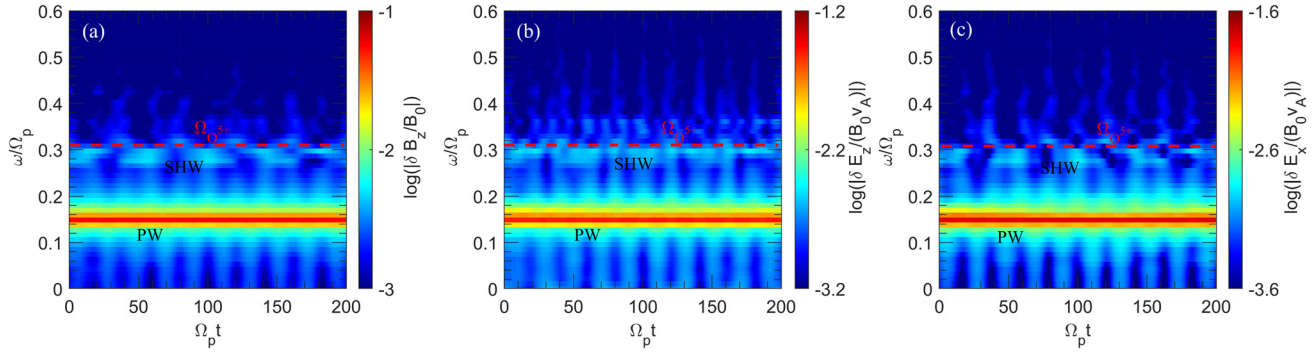

FIG. 2. (a) The $\omega-t$ spectrogram of perpendicular fluctuating magnetic fields $\delta B_z/B_0$ obtained by sliding short time Fourier analysis with a window size of 300 Ω_p^{-1}, (b) the $\omega-t$ spectrogram of perpendicular fluctuating electric fields $\delta E_z/(B_0V_A)$, and (c) the $\omega-t$ spectrogram of perpendicular fluctuating electric fields $\delta E_x/(B_0V_A)$. The pump wave, its second harmonic wave, and its third harmonic wave are denoted by "PW," "SHW," and "THW," respectively. The cyclotron frequency of O^{5+} with $\omega = 0.3125\,\Omega_P$ is marked with the red dashed line.

where the bracket $\langle \ldots \rangle$ denotes an average over 50 Ω_p^{-1} intervals, $\boldsymbol{k}_{HW} = \boldsymbol{k}_{Ex} + \boldsymbol{k}_{Ez}$ is the wavenumber of the wave generated by the coupling of δE_z and δE_x, and superscript * denotes the complex conjugate. According to this definition, the bc index will be close to 1.0 when these three components satisfy the resonant condition, i.e., $\boldsymbol{k}_{HW} = \boldsymbol{k}_{Ex} + \boldsymbol{k}_{Ez}$. The bicoherence index presented for $\Omega_p t = 200 \sim 250$ is illustrated in Fig. 3; point #1 located at $(k_{E_x} c/\omega_{pp}, k_{E_z} c/\omega_{pp}) \approx (0.17, 0.17)$ with a value of 0.84 indicates the coupling among the δE_x component and the δE_z component of the fundamental wave. Point #2 at $(k_{E_x} c/\omega_{pp}, k_{E_z} c/\omega_{pp}) \approx (0.34, 0.17)$ with a value of 0.94 indicates the coupling within the δE_z component of the fundamental wave and the δE_x component of the second harmonic wave. Point #3 in Fig. 3 with the position $(k_{E_x} c/\omega_{pp}, k_{E_z} c/\omega_{pp}) \approx (0.17, 0.34)$ with a value of 0.89 indicates the coupling among the δE_x component of the fundamental wave and the δE_z component of the second harmonic wave. Similarly, points #4, #5, and #6 located at $(k_{E_x} c/\omega_{pp}, k_{E_z} c/\omega_{pp}) \approx (0.17, 0.51)$, $(0.34, 0.34)$, and $(0.51, 0.17)$ imply that the fourth harmonic wave is generated via the coupling among the electrostatic component and electromagnetic component of low-frequency waves. All of these points have the value $bc > 0.7$, which convincingly demonstrates that the harmonic Alfvén waves are generated by the coupling among the electric component δE_x and the electromagnetic component δE_z. The mechanism to excite harmonic Alfvén waves is similar to that for whistler waves, which has been studied with both satellite observations and theoretical works.[40–43]

The wave-wave coupling process generates higher frequency waves, which makes the wave-particle resonant condition easier to be satisfied for heavy ions. In the following, we will discuss the cyclotron resonant heating of heavy ions. The parallel and perpendicular temperatures are calculated using the following procedure:[13] first, we calculate the parallel temperature $T_{j||} = (m_j/k_B)\langle (v_{||} - \langle v_{||} \rangle)^2 \rangle$ and the perpendicular temperature $T_{j\perp} = (m_j/2k_B)\langle (v_{\perp 1} - \langle v_{v_{\perp 1}} \rangle)^2 + (v_{\perp 2} - \langle v_{v_{\perp 2}} \rangle)^2 \rangle$ for ion species j in every grid cell (the brackets $\langle\rangle$ denote an average over one grid cell), where $v_{||} = v_x \cos\theta_{kB} + v_y \sin\theta_{kB}$, $v_{\perp 1} = -v_x \sin\theta_{kB} + v_y \cos\theta_{kB}$, and $v_{\perp 2} = v_z$, with θ_{kB} being the wave normal angle and k_B the Boltzmann constant. Then, the temperatures are averaged over all grids. Using this method, the effects of the bulk velocity at each location on the thermal temperature can be eliminated. The temperature profiles of protons and O^{5+} are displayed in Fig. 4(a); the perpendicular temperature of protons (black dashed line), the parallel temperature of protons (black solid line), and the parallel temperature of O^{5+} (red dashed line) are nearly unchanged. Meanwhile, the perpendicular temperature of O^{5+} (red solid line) increases up to 2.3 times of its initial value. This preferential heating O^{5+} in the perpendicular direction is consistent with previous observations.[6–8] Figures 4(b)–4(d) show the velocity distribution of O^{5+} at three different moments, including (b) the initial velocity distribution of O^{5+}, (c) the velocity distribution at $t = 150\,\Omega_p^{-1}$, and (d) the velocity distribution at $t = 400\,\Omega_p^{-1}$. In the figures, the bulk velocity has been subtracted for eliminating the contribution of the bulk velocity, and the parallel velocity $v_{||} = v_x \cos\theta_{kB} + v_y \sin\theta_{kB}$ and the perpendicular velocity $v_\perp = \sqrt{(v_{\perp 1}^2 + v_{\perp 2}^2)/2}$ ($v_{\perp 1} = -v_x \sin\theta_{kB} + v_y \cos\theta_{kB}$, and $v_{\perp 2} = v_z$). O^{5+} are scattered mainly in the perpendicular direction, and the scattering occurs dominantly for particles with $v_{||} < 0$. This can be interpreted with the cyclotron resonant relation of a left-handed polarized wave, $\omega - k_{||} v_{||} = \Omega_{O^{5+}}$. For the second harmonic Alfvén wave with $\omega = 2\omega_0 \approx 0.30\,\Omega_p$ and $k = 2k_0 \approx 0.34 d_i^{-1}$, the resonant velocity is $v_{||} \approx -0.04 v_A$. This indicates that the resonant interaction with O^{5+} occurs mainly for particles with parallel velocities close to $-0.04 v_A$. Nonlinear trapping/acceleration theory[44,45] can present a more detailed physical process; what is more, the range of velocities of accelerated ions can be estimated via this theory. Therefore, we use this concept in our manuscript to calculate how far perpendicular and parallel velocity components of ions may reach the maximum. According to previous work,[44,45] the trapping half-width, which is due to the fact that the perturbation shifts the particles away from resonance, is $\Delta v_{||} \approx 0.07 v_A$ in this condition. Thus, the range of parallel velocity components of accelerated ions is estimated to be $-0.11 v_A < v_{||} < 0.03 v_A$. For test particles, the effect of particles on waves can be ignored, and the quantity $H = (v_{||} - v_p)^2 + v_\perp^2$ remains constant during the heating of heavy ions, where $v_p = \frac{\omega}{k} \approx 0.88 v_A$ is the phase velocity of the second harmonic wave. Therefore, for particles located at $(v_{||0}, v_{\perp 0}) = (-0.04 v_A, 0.3 v_A)$ initially, the maximum perpendicular velocity calculated via $(v_{||0} - v_p)^2 + v_{\perp 0}^2 = (v_{||1} - v_p)^2 + v_{\perp \max}^2$ (where $v_{||1} = 0.03 v_A$ is the maximum parallel velocity of trapping particles) is $v_{\perp \max} \approx 0.46 v_A$; therefore, the range of perpendicular velocities is $-0.46 v_A < v_\perp < 0.46 v_A$. This result agrees well with our simulation results.

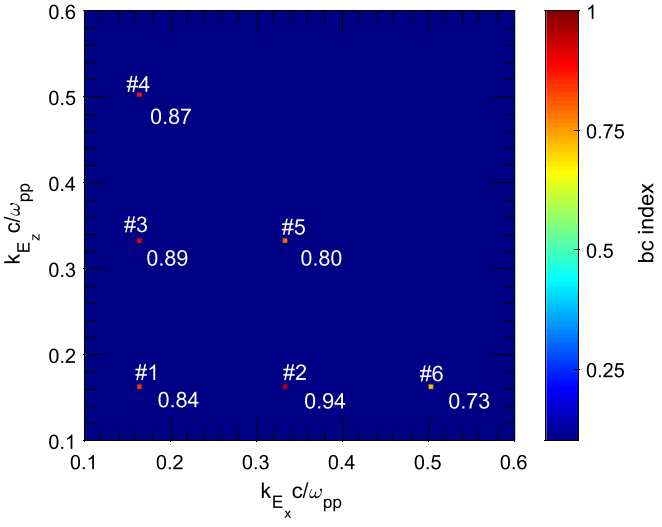

FIG. 3. The bicoherence indices among the electric components δE_x and δE_z for the timespan $\Omega_p t = 200 \sim 250$.

As a comparison, run 2 with the propagating angle $\theta = 0^0$ is performed. According to Eq. (3), the fluctuating density and associated electric field δE_x will be zero; in principle, no wave-wave coupling occurs and only the pump wave appears in this condition. This can be illustrated by the $\omega - t$ spectrograms of δB_z and δE_z illustrated in Figs. 5(a) and 5(b), respectively. As shown in Figs. 5(a) and 5(b), only pump wave (PW) with $\omega_0 \approx 0.15\,\Omega_p$ appears; the red dashed line denotes the gyrofrequency of O^{5+} with $\Omega_{O^{5+}} = 0.3125\,\Omega_p$. The temperature evolution for run 2 is shown in Fig. 5(c); the heavy ions cannot be heated because there are no harmonic waves in this condition and the frequency of the pump wave is too low relative to heat ions.

It is necessary to perform run 3 to simulate the real wave fields having a wide spectral range. Wave fields of run 3 are composed of five Alfvén waves with the same propagating angle ($\theta = 20^\circ$), and amplitudes

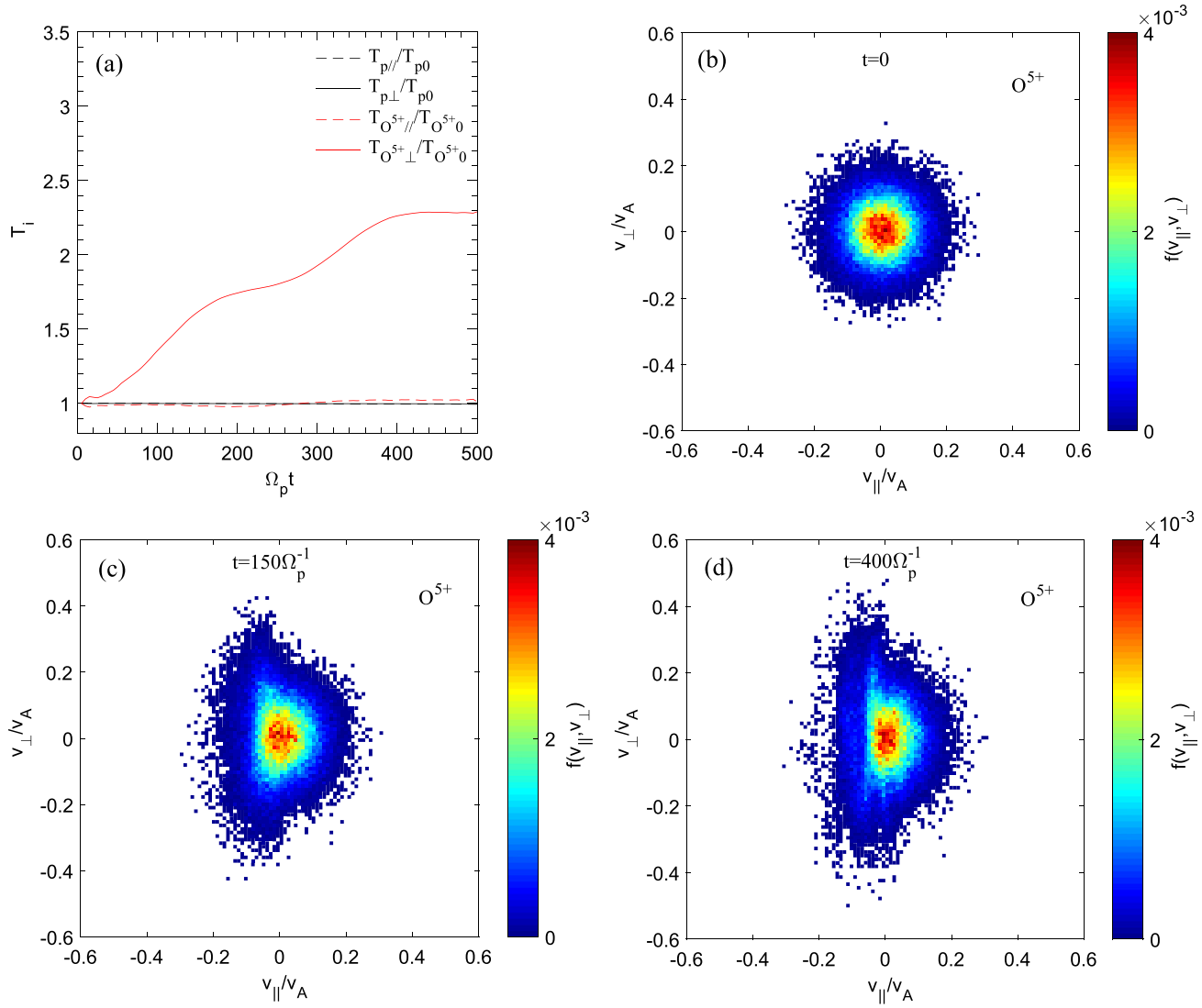

FIG. 4. The evolution of temperature and the velocity distribution of heavy ions for run 1. (a) The temporal profiles for the perpendicular temperature (solid line) and parallel temperature (dashed line) of O^{5+}(black) and protons (red), respectively. (b) The initial velocity distribution of O^{5+} at $t = 0\,\Omega_p^{-1}$, (c) the velocity distribution $f(v_{||}, v_\perp)$ at $t = 150\,\Omega_p^{-1}$, and (d) $f(v_{||}, v_\perp)$ at $t = 400\,\Omega_p^{-1}$. Subscripts || and ⊥ denote the parallel and perpendicular directions relative to the ambient magnetic field.

of these five waves are assumed to be the same; the parameters are shown in Table I. The $k - t$ spectrograms of electromagnetic fields are shown in Fig. 6, including (a) the $k - t$ spectrogram of magnetic field component δB_z, (b) the $k - t$ spectrogram of fluctuating electric field component δE_z, and (c) the $k - t$ spectrogram of fluctuating electric field δE_x. The spectra in Fig. 6 are much more complicated than those in Fig. 1 because the coupling between the electrostatic components and electromagnetic components of different waves also emerges in this condition. The $k - t$ spectra in Fig. 6 are divided into five parts denoted by "I," "II," "III," "IV," and "V," respectively. The red-colored lines in part I represent the pump waves, and lines in part II, part III, and part IV correspond to the second harmonic waves, the third harmonic waves, and the fourth harmonic waves, respectively. Lines in part V, which do not appear in Fig. 1, denote waves generated by the subtraction of pump waves.

The evolution of the temperature of protons and O^{5+} for run 3 is illustrated in Fig. 7(a). The perpendicular temperature of protons (black dashed line), the parallel temperature of protons (black solid line), and the parallel temperature of O^{5+}(red dashed line) are nearly unchanged. Meanwhile, the perpendicular temperature of O^{5+}(red solid line) increases up to about 4 times compared to its initial state. Compared with Fig. 4(a), the perpendicular heating of heavy ions is much more effective than that for the monochromatic wave situation. This difference of perpendicular heating is due to that more particles satisfy the cyclotron resonant condition for wave fields composed of several waves. This can be illustrated by the evolution of distribution of O^{5+} shown in Figs. 7(b)–7(d). Figures 7(b)–7(d) display the velocity distribution of O^{5+} at three different moments, including (b) the initial velocity distribution of O^{5+}, (c) the velocity distribution at

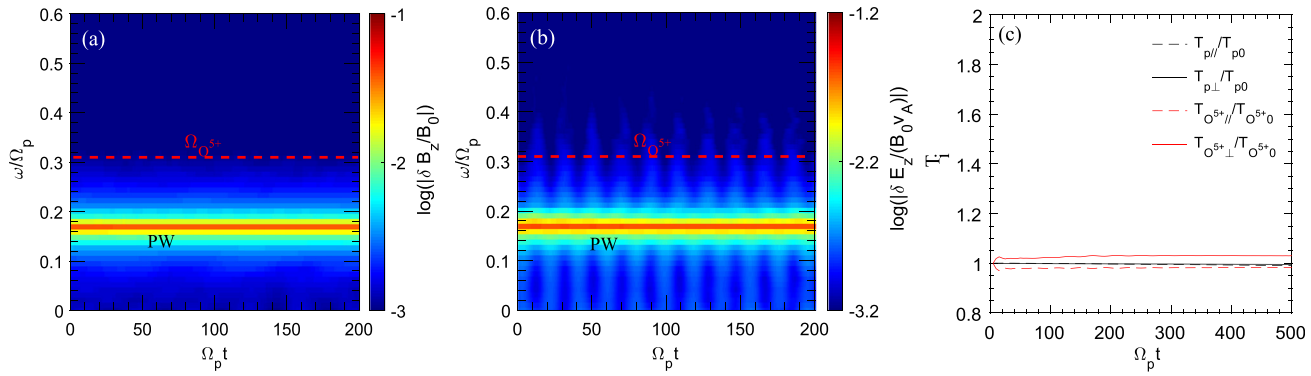

FIG. 5. (a) The temporal profiles for the perpendicular temperature (solid line) and parallel temperature (dashed line) of O^{5+}(black) and protons (red) for run 2, respectively, and (b) the $\omega - t$ spectrogram of perpendicular fluctuating electric fields $\delta B_z/(B_0 V_A)$ obtained by sliding short time Fourier analysis with a window size of 300 Ω_p^{-1} for run 2, and (c) the $\omega - t$ spectrogram of perpendicular fluctuating electric fields $\delta E_z/(B_0 V_A)$ for run 2. The pump wave is denoted by "PW." The cyclotron frequency of O^{5+} with $\omega = 0.3125\,\Omega_p$ is marked with the red dashed line.

$t = 150\Omega_p^{-1}$, and (d) the velocity distribution at $t = 400\Omega_p^{-1}$. Similar to Figs. 4(b)–7(d), O^{5+} are scattered mainly in the perpendicular direction, but all particles not only particles with $v_{||} < 0$ are scattered for run 3. This can be interpreted with cyclotron resonance. According to the cyclotron resonance relation $v_{||} = (\omega - \Omega_{O^{5+}})/k_{||}$, particles with $v_{||} < 0$ can be scattered for the condition $\omega < \Omega_{O^{5+}}$ and vice versa. Therefore, for the second harmonic wave fields having broadband frequencies below $\Omega_{O^{5+}}$ and above $\Omega_{O^{5+}}$, all the ions can be scattered in the perpendicular direction.

IV. CONCLUSIONS AND DISCUSSION

Based on the 1-D hybrid simulations, the generation of harmonic Alfvén waves and associated heavy ion heating are investigated in this paper. We find that the fluctuating densities and associated electrostatic fluctuations occur when Alfvén waves propagate obliquely with respect to the ambient magnetic field. Furthermore, through the corresponding bicoherence index, we demonstrated the harmonic Alfvén waves can be generated via the coupling among the electrostatic components (or equivalently the density fluctuations) and the electromagnetic components of the Alfvén waves. The parallel propagating monochromatic Alfvén wave is also investigated as a comparison, and we find that it cannot cause harmonic waves because of no electrostatic component in this condition. In addition, through the investigation of wave fields composed of several waves, we find that the perpendicular heating of heavy ions is more efficient because more ions can be scattered due to the broadband frequencies of second-harmonic waves.

The generation of harmonic Alfvén waves has been *in situ* observed by Chen *et al.*[1] in the magnetosphere with Van Allen Probes, and the preferentially perpendicular heating of heavy ions by the harmonic Alfvén waves is also demonstrated. This is consistent with our simulations; the perpendicular velocity of heavy ions scatters severely around the velocity satisfying cyclotron resonant relation $\omega - k_{||} v_{||} = \Omega_{O^{5+}}$. Therefore, the generation mechanism of harmonic Alfvén waves investigated in this paper can potentially shed light on the energy cascade from low-frequency Alfvén waves to high-frequency Alfvén waves, which can efficiently heat heavy ions via cyclotron resonant scattering. It may pave a new way for us to

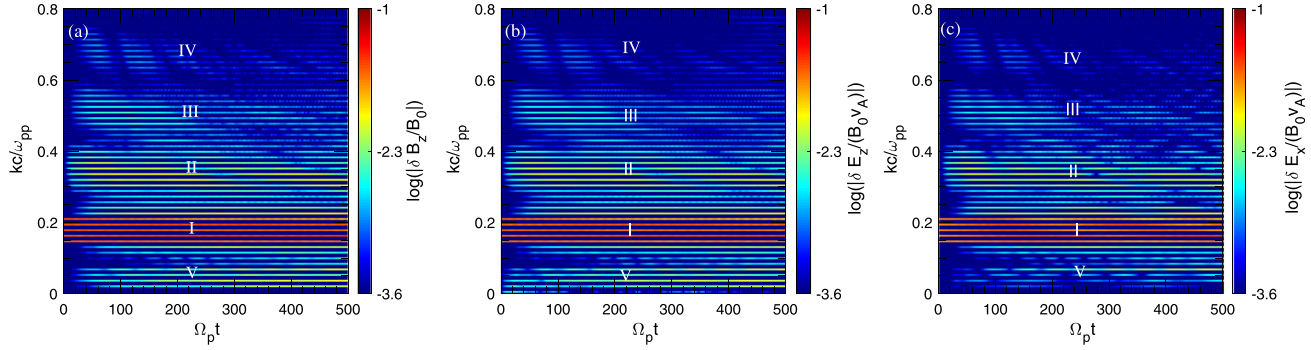

FIG. 6. The $k - t$ spectra of electromagnetic fields for run 3. (a) The $k - t$ spectrogram of perpendicular fluctuating magnetic fields ($\delta B_z/B_0$) obtained from the fast Fourier transform, (b) the $k - t$ spectrogram of perpendicular fluctuating electric fields $\delta E_z/(B_0 V_A)$ obtained from the fast Fourier transform, and (c) the $k - t$ spectrogram of parallel fluctuating electric fields $\delta E_x/(B_0 V_A)$. In all panels, the spectrogram is divided into five parts denoted by "I," "II," "III," "IV," and "V," respectively. The red colored lines in part I represent the pump waves; part II, part III, and part IV mainly correspond to the second harmonic waves, the third harmonic waves, and the fourth harmonic waves, respectively. Lines in the part denoted with "V" are waves generated by the subtraction of pump waves.

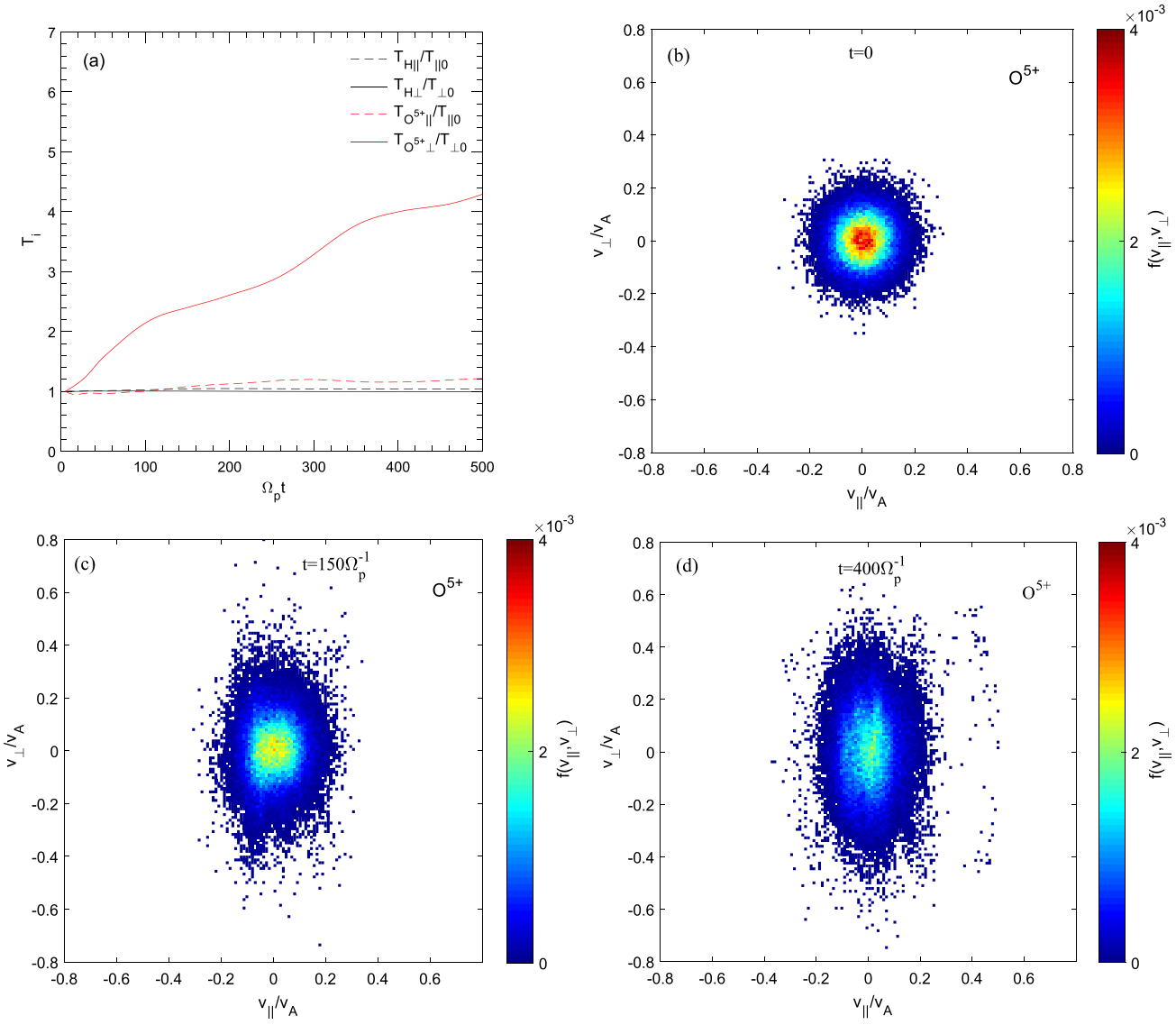

FIG. 7. The evolution of temperature and the velocity distribution of heavy ions for run 3. (a) The temporal profiles for the perpendicular temperature (solid line) and parallel temperature (dashed line) of O^{5+}(black) and protons (red), respectively. (b) The initial velocity distribution of O^{5+} at $t = 0\,\Omega_p^{-1}$, (c) the velocity distribution $f(v_{||}, v_\perp)$ at $t = 150\,\Omega_p^{-1}$, and (d) $f(v_{||}, v_\perp)$ at $t = 400\,\Omega_p^{-1}$. Subscripts || and ⊥ denote the parallel and perpendicular directions relative to the ambient magnetic field.

interpret the corona heating of the corona because of the ubiquitous existence of Alfvén waves in the solar corona.

ACKNOWLEDGMENTS

This work was supported by the NSFC (Grant Nos. 41527804 and 41774169) and the Key Research Program of Frontier Sciences, CAS (No. QYZDJ-SSW-DQC010). Simulations were performed on TH-1A at the National Super-Computer Center in Tianjin.

REFERENCES

[1]H. Chen, X. Gao, Q. Lu, and S. Wang, Astrophys. J. **859**, 120 (2018).
[2]L. F. Burlaga, Space Sci. Rev. **39**, 225 (1984).
[3]R. Bruno and V. Carbone, Living Rev. Sol. Phys. **2**, 4 (2005).
[4]E. Marsch, Living Rev. Sol. Phys. **3**, 1 (2006).
[5]J. V. Hollweg, Philos. Trans. R. Soc., A. **364**, 505 (2006).
[6]J. L. Kohl, G. Noci, S. R. Granmer, and J. C. Raymond, Astron. Astrophys. Rev. **13**, 31 (2006).
[7]K. Wilhelm, E. Marsch, B. N. Dwivedi, and U. Feldman, Space Sci. Rev. **133**, 103 (2007).
[8]S. R. Cranmer, A. V. Panasyuk, and J. L. kohl, Astrophys. J. **678**, 1480 (2008).
[9]L. Dolla and J. Solomon, Astron. Astrophys. **483**, 271 (2008).
[10]S. Tomczyk, S. W. Mclntosh, S. L. Keil, P. G. Judge, T. Schad, D. H. Seeley, and J. Edmondson, Science **317**, 1192 (2007).
[11]L. Chen, Z. H. Lin, and R. B. White, Phys. Plasmas **8**, 4713 (2001).
[12]Q. M. Lu and L. Chen, Astrophys. J. **704**, 743 (2009).

[13]Q. M. Lu and X. Li, Phys. Plasmas **14**, 042303 (2007).
[14]S. Jicheng, G. Xinliang, L. Quanming, and W. Shui, Plasma Sci. Technol. **16**, 919 (2014).
[15]C. Y. Tu and E. Marsch, Sol. Phys. **171**, 363 (1997).
[16]J. V. Hollweg, J. Geophys. Res. **104**, 24781, https://doi.org/10.1029/1999JA900300 (1999).
[17]S. R. Cranmer, Astrophys. J. **532**, 1197 (2000).
[18]P. A. Isenberg, M. A. Lee, and J. V. Hollweg, J. Geophys. Res. **106**, 5649, https://doi.org/10.1029/2000JA000099 (2001).
[19]S. Sridhar and P. Goldreich, Astrophys. J. **432**, 612 (1994).
[20]P. Goldreich and S. Sridhar, Astrophys. J. **438**, 763 (1995).
[21]E. Quataert, Astrophys. J. **500**, 978 (1998).
[22]B. J. Vasquez, S. A. Markovskii, and B. D. G. Chandran, Astrophys. J. **788**, 178 (2014).
[23]J. V. Shebalin, W. H. Matthaeus, and D. Montgomery, J. Plasma Phys. **29**, 525 (1983).
[24]C. S. Ng and A. Bhattacharjee, Astrophys. J. **465**, 845 (1996).
[25]L. J. Milano, W. H. Matthaeus, P. Dmitruk, and D. C. Montgomery, Phys. Plasmas **8**, 2673 (2001).
[26]S. Oughton, P. Dmitruk, and W. H. Matthaeus, Phys. Plasmas **11**, 2214 (2004).
[27]J. V. Hollweg, J. Astrophys. Astron. **29**, 217 (2008).
[28]S. R. Cranmer, A. A. van Ballegooijen, and R. J. Edgar, Astrophys. J., Suppl. Ser. **171**, 520 (2007).
[29]P. Dmitruk, W. H. Matthaeus, N. Seenu, and M. R. Brown, Astrophys. J. **597**, L81 (2003).
[30]M. Wan, W. Matthaeus, V. Roytershteyn, H. Karimabadi, T. Parashar, P. Wu, and M. Shay, Phys. Rev. Lett. **114**, 175002 (2015).
[31]W. H. Matthaeus, D. J. Mullan, P. Dmitruk, L. Milano, and S. Oughton, Nonlinear Processes Geophys. **10**, 93–100 (2003).
[32]D. Winske, Space Sci. Rev. **42**, 53 (1985).
[33]K. B. Quest, J. Geophys. Res. **93**, 9649, https://doi.org/10.1029/JA093iA09p09649 (1988).
[34]Q. M. Lu and S. Wang, Geophys. Res. Lett. **32**, L03111, https://doi.org/10.1029/2004GL021508 (2005).
[35]S. J. Bame, J. R. Asbridge, W. C. Feldman, M. D. Montgomery, and P. D. Kearney, Sol. Phys. **43**, 463–473 (1975).
[36]Y. Chen, R. Esser, and Y. Q. Hu, J. Geophys. Res. **107**(A11), 1368, https://doi.org/10.1029/2002JA009341 (2002).
[37]B. P. van Milligen, E. Sánchez, T. Estrada, C. Hidalgo, B. Brañas, B. Carreras, and L. García, Phys. Plasmas **2**, 3017 (1995).
[38]Y. Nariyuki and T. Hada, Nonlinear Processes Geophys. **13**, 425 (2006).
[39]Y. Nariyuki, T. Hada, and K. Tsubouchi, J. Geophys. Res. **114**, A07102, https://doi.org/10.1029/2009JA014178 (2009).
[40]X. Gao, Y. Ke, Q. Lu, L. Chen, and S. Wang, Geophys. Res. Lett. **44**, 618, https://doi.org/10.1002/2016GL072251 (2017).
[41]X. Gao, Q. Lu, J. Bortnik, W. Li, L. Chen, and S. Wang, Geophys. Res. Lett. **43**, 2343, https://doi.org/10.1002/2016GL068313 (2016).
[42]H. Chen, X. Gao, Q. Lu, Y. Ke, and S. Wang, J. Geophys. Res. **122**, 10,448, https://doi.org/10.1002/2017JA024513 (2017).
[43]X. Gao, Q. Lu, and S. Wang, AIP Adv. **8**, 055003 (2018).
[44]H. Karimabadi, K. Akimoto, N. Omidi, and C. R. Menyuk, Phys. Fluids B **2**(3), 606 (1990).
[45]Karimabadi, H. D. Krauss-Varban, and T. Terasawa, J. Geophys. Res. **97**, 13853, https://doi.org/10.1029/92JA00997 (1992).